

Supplemental Material

**Cu/ZnO Nanocatalysts in Response to Environmental Conditions:
Surface Morphology, Electronic Structure, Redox State and CO₂ Activation**

Luis Martínez-Suárez, Johannes Frenzel* and Dominik Marx

Lehrstuhl für Theoretische Chemie, Ruhr-Universität Bochum, 44780 Bochum, Germany

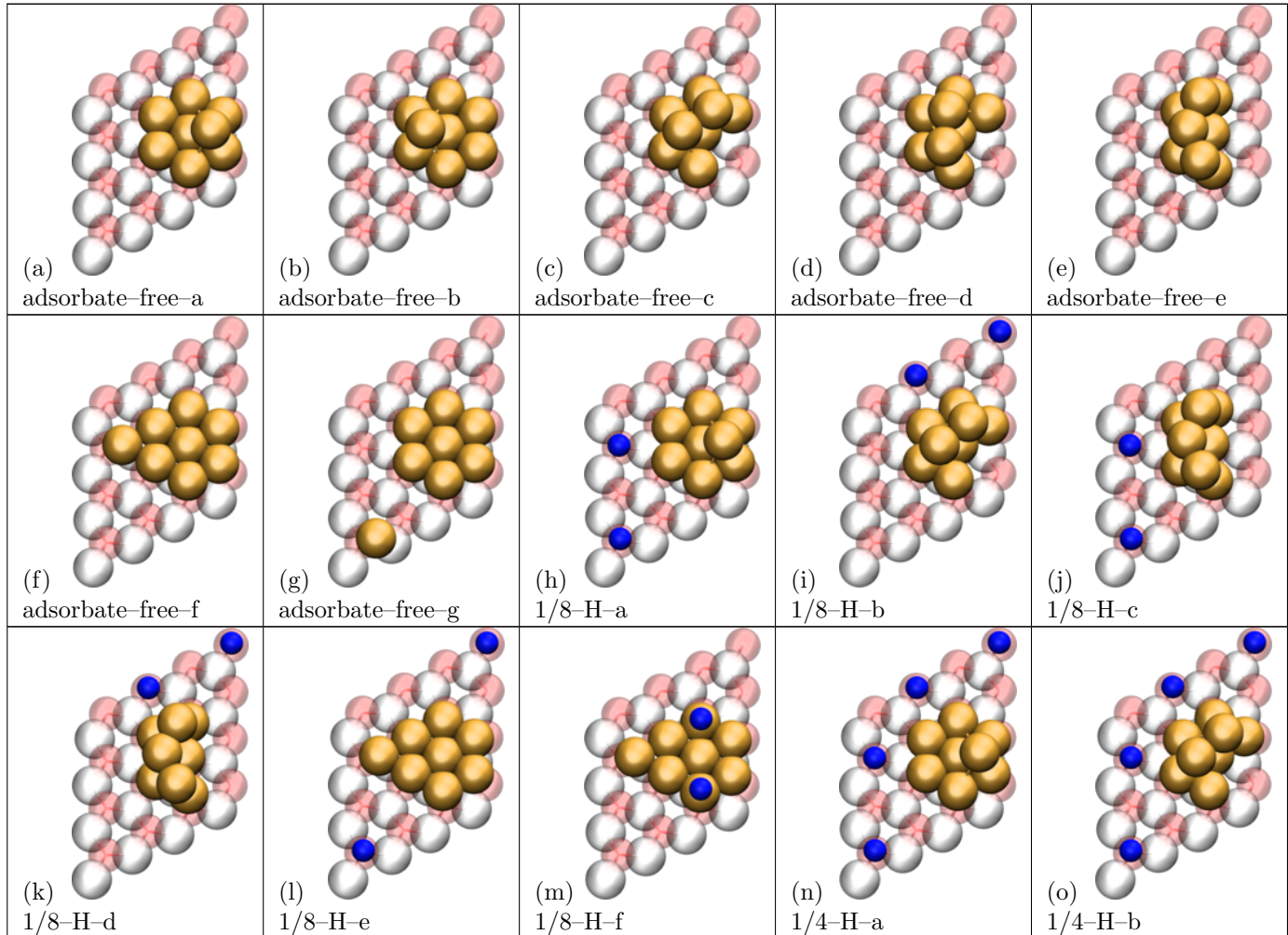
E-mail: johannes.frenzel@theochem.rub.de;
Phone: ++49 (0)234 322 6750,
Fax : ++49 (0)234 321 4045

1 Supported nanocatalyst structures

The nuclear positions of all structures were relaxed until the largest component of the residual forces remained below a threshold of 6 meV/Å. Herein, the k -space was sufficiently sampled by the Γ point, only. In Tab. S2 the relative energies of all $\text{Cu}_8/\text{ZnO}(000\bar{1})$ catalyst slab models are given w.r.t. the most stable adsorbate-free and defect-free Cu/ZnO model (see Tab. S1f). These energies were calculated using a increased k -grid,¹ which reproduced the total energies within an accuracy $> 2 \text{ mHa}$ upon increase the grid size from $2 \times 2 \times 1$ to $4 \times 4 \times 1$.

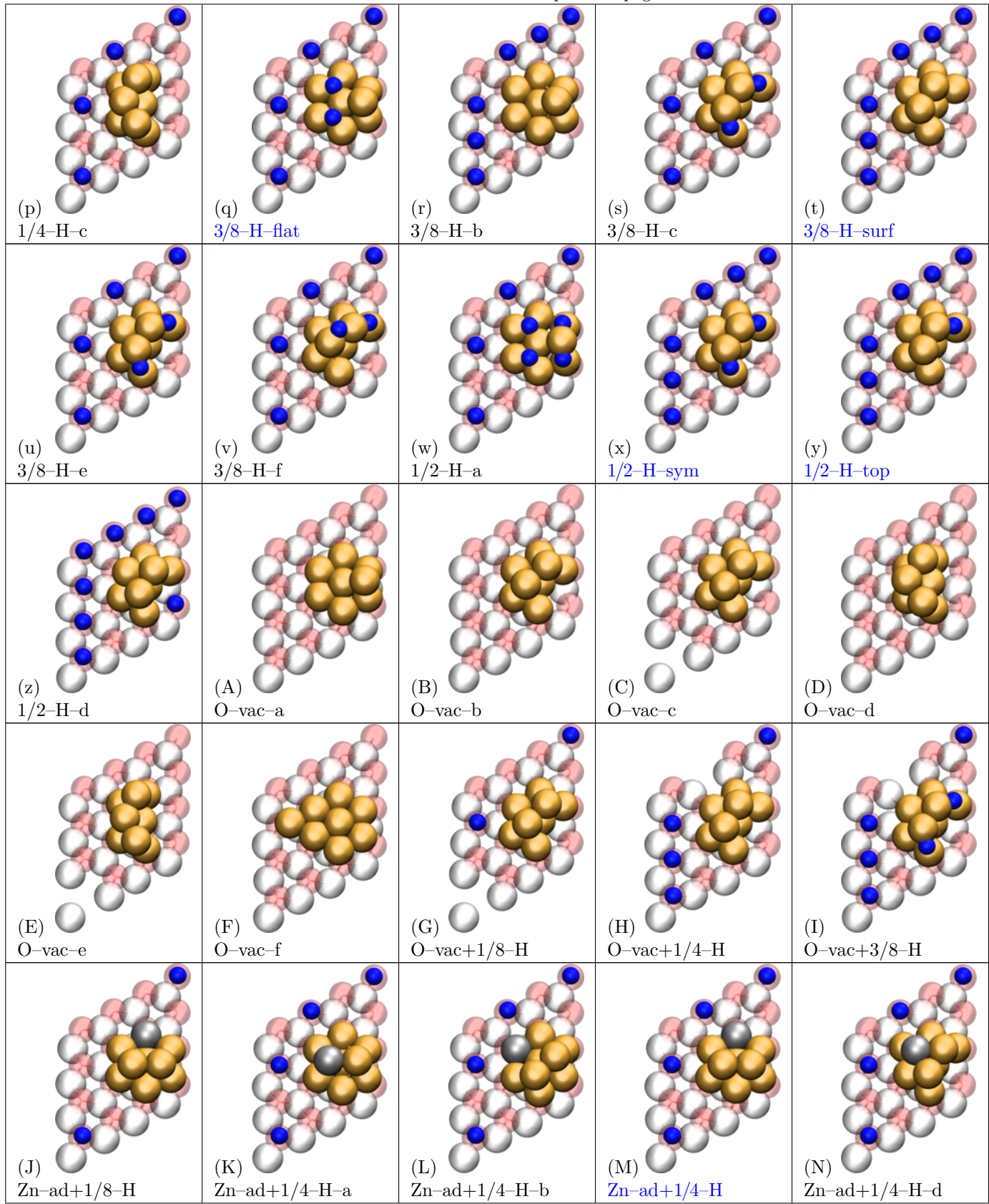
Tab. S1 summarizes the optimized atomic structures of all 58 putative $\text{Cu}_8/\text{ZnO}(000\bar{1})$ slab models which have been considered throughout our study. The corresponding relative energies are given in Tab. S2. In addition, this table the change in the number of individual surface adspecies is given with respect to the adsorbate-free free catalyst surface, i.e. hydrogen atoms, oxygen atoms and zinc adatoms. Throughout this supporting information we use the following color code for the atoms: Zn (silver-gray), O (red), Cu (copper), C (cyan), and H (blue) for the adsorbates and light colors for the $\text{ZnO}(000\bar{1})$ support, i.e. Zn (light silver-gray) and O (light red). In all figures we only show the top layer of ZnO , the Cu_8 cluster and the adsorbates (H, Zn, ZnO , O atoms, and CO_2 molecule) of the Cu/ZnO models which consist of $4 \times 4 \times 4 \text{ ZnO}(000\bar{1})$ surface slab. O vacancies have been considered only in the top surface layer (see Tab. S1A through Tab. S1I and Tab. S1V). In several cases the site of the vacancy is below the center of Cu_8 cluster and therefore are hidden to the eye (see Tab. S1A, Tab. S1B, Tab. S1D and Tab. S1F). Blue labels are used to indicate structures that also appear in figures of the main paper.

Table S1 $\text{Cu}_8/\text{ZnO}(000\bar{1})$ surface structures: Top view of the investigated catalyst morphologies. The color code for the atoms is: Zn (silver-gray), O (red), Cu (copper), and H (blue) for the adsorbates and light colors for the $\text{ZnO}(000\bar{1})$ support, i.e. Zn (light silver-gray) and O (light red). Models (A) through (I) and (V) have an O vacancy site present in the top O surface layer. Note that this vacancy is below the Cu_8 cluster in subfigures (A), (B), (D,) and (F), and therefore hidden to the eyes. Blue labels indicate structures that also appear in figures of the main paper.



Continued on next page

Table S1 – continued from previous page



Continued on next page

Table S1 – continued from previous page

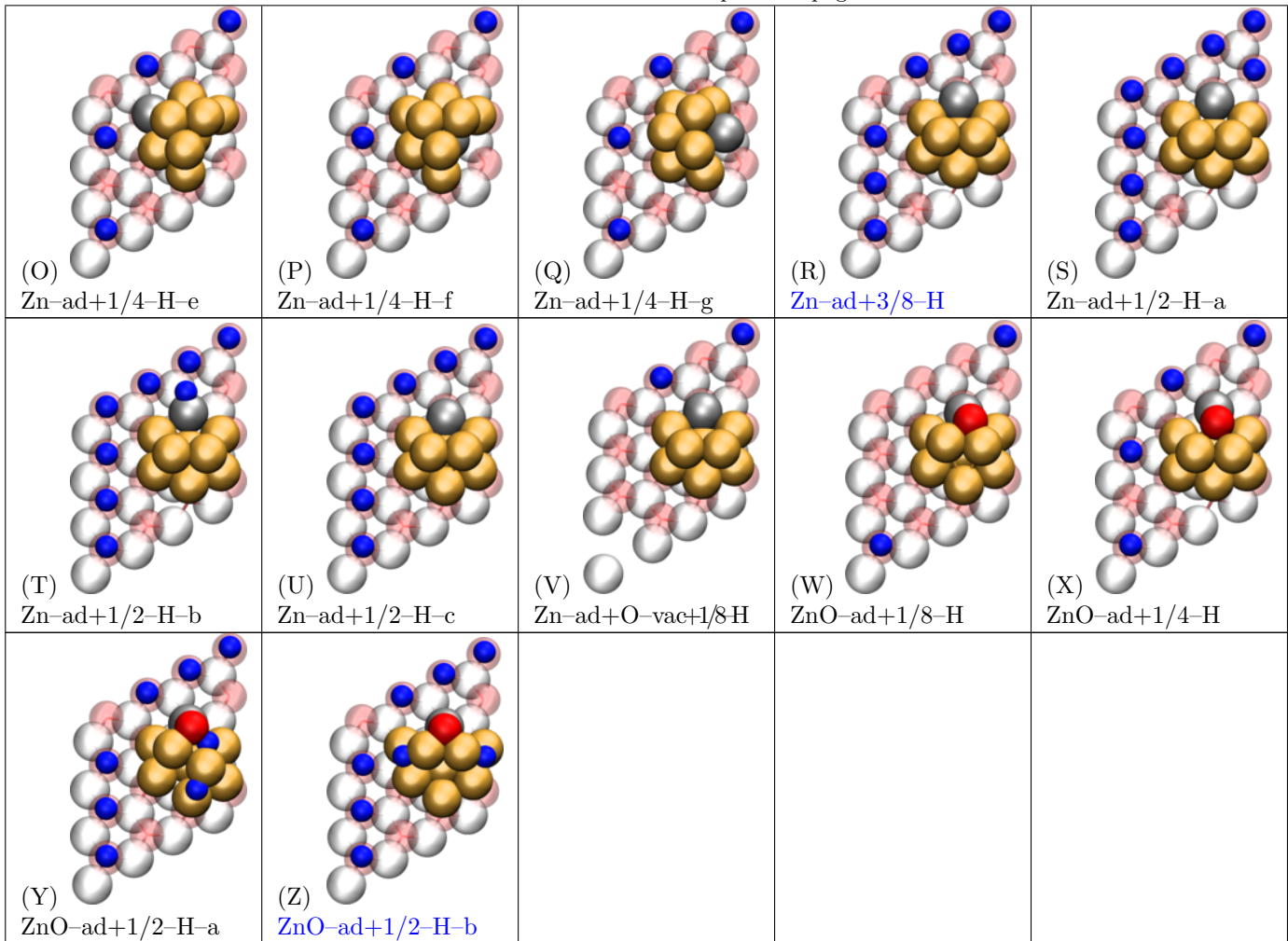


Table S2 Thermodynamic stability and structural changes of Cu₈/ZnO(0001̄) nanocatalyst surface structures. The differences total energy ΔE are calculated relative to the total energy of the adsorbate-free-f structure, i. e. using $4 \times 4 \times 1$ and $1 \times 1 \times 1$ k -point meshes. ΔN_X is the difference in the number of atoms of adsorbate species X on the Cu₈/ZnO(0001̄) surface with respect to the adsorbate-free-f structure (see Tab. S1f). Blue labels indicate structures that also appear in figures of the main paper.

| catalyst model | $\Delta E^{4 \times 4 \times 1}$ /Ha | $\Delta E^{1 \times 1 \times 1}$ /Ha | ΔN_O | ΔN_H | ΔN_{Zn} | structure |
|-------------------|--------------------------------------|--------------------------------------|--------------|--------------|-----------------|-----------|
| adsorbate-free-a | 0.005 | 0.001 | 0 | 0 | 0 | Tab. S1a |
| adsorbate-free-b | 0.005 | 0.002 | 0 | 0 | 0 | Tab. S1b |
| adsorbate-free-c | 0.012 | 0.002 | 0 | 0 | 0 | Tab. S1c |
| adsorbate-free-d | 0.012 | 0.002 | 0 | 0 | 0 | Tab. S1d |
| adsorbate-free-e | 0.045 | 0.035 | 0 | 0 | 0 | Tab. S1e |
| adsorbate-free-f | 0.000 | 0.000 | 0 | 0 | 0 | Tab. S1f |
| adsorbate-free-g | 0.011 | 0.011 | 0 | 0 | 0 | Tab. S1g |
| 1/8-H-a | -1.310 | -1.306 | 0 | 2 | 0 | Tab. S1h |
| 1/8-H-b | -1.306 | -1.305 | 0 | 2 | 0 | Tab. S1i |
| 1/8-H-c | -1.272 | -1.270 | 0 | 2 | 0 | Tab. S1j |
| 1/8-H-d | -1.270 | -1.268 | 0 | 2 | 0 | Tab. S1k |
| 1/8-H-e | -1.316 | -1.311 | 0 | 2 | 0 | Tab. S1l |
| 1/8-H-f | -1.167 | -1.164 | 0 | 2 | 0 | Tab. S1m |
| 1/4-H-a | -2.611 | -2.604 | 0 | 4 | 0 | Tab. S1n |
| 1/4-H-b | -2.620 | -2.612 | 0 | 4 | 0 | Tab. S1o |
| 1/4-H-c | -2.582 | -2.574 | 0 | 4 | 0 | Tab. S1p |
| 3/8-H-flat | -3.847 | -3.840 | 0 | 6 | 0 | Tab. S1q |
| 3/8-H-b | -3.834 | -3.830 | 0 | 6 | 0 | Tab. S1r |
| 3/8-H-c | -3.828 | -3.821 | 0 | 6 | 0 | Tab. S1s |

Continued on next page

Table S2 – continued from previous page

| catalyst model | $\Delta E^{4 \times 4 \times 1}$ /Ha | $\Delta E^{1 \times 1 \times 1}$ /Ha | ΔN_O | ΔN_H | ΔN_{Zn} | structure |
|-----------------------|--------------------------------------|--------------------------------------|--------------|--------------|-----------------|-----------|
| 3/8-H-surf | -3.840 | -3.840 | 0 | 6 | 0 | Tab. S1t |
| 3/8-H-e | -3.828 | -3.821 | 0 | 6 | 0 | Tab. S1u |
| 3/8-H-f | -3.818 | -3.811 | 0 | 6 | 0 | Tab. S1v |
| 1/2-H-a | -5.043 | -5.036 | 0 | 8 | 0 | Tab. S1w |
| 1/2-H-sym | -5.026 | -5.040 | 0 | 8 | 0 | Tab. S1x |
| 1/2-H-top | -5.046 | -5.043 | 0 | 8 | 0 | Tab. S1y |
| 1/2-H-d | -5.019 | -5.040 | 0 | 8 | 0 | Tab. S1z |
| O-vac-a | 16.025 | 16.024 | -1 | 0 | 0 | Tab. S1A |
| O-vac-b | 16.050 | 16.050 | -1 | 0 | 0 | Tab. S1B |
| O-vac-c | 15.994 | 15.993 | -1 | 0 | 0 | Tab. S1C |
| O-vac-d | 16.081 | 16.076 | -1 | 0 | 0 | Tab. S1D |
| O-vac-e | 16.025 | 16.024 | -1 | 0 | 0 | Tab. S1E |
| O-vac-f | 16.022 | 16.020 | -1 | 0 | 0 | Tab. S1F |
| O-vac+1/8-H | 14.680 | 14.684 | -1 | 2 | 0 | Tab. S1G |
| O-vac+1/4-H | 13.468 | 13.464 | -1 | 4 | 0 | Tab. S1H |
| O-vac+3/8-H | 12.276 | -3.811 | -1 | 6 | 0 | Tab. S1I |
| Zn-ad+1/8-H | -64.641 | -64.634 | 0 | 2 | 1 | Tab. S1J |
| Zn-ad+1/4-H-a | -65.928 | -65.917 | 0 | 4 | 1 | Tab. S1K |
| Zn-ad+1/4-H-b | -65.945 | -65.934 | 0 | 4 | 1 | Tab. S1L |
| Zn-ad+1/4-H | -65.948 | -65.937 | 0 | 4 | 1 | Tab. S1M |
| Zn-ad+1/4-H-d | -65.924 | -65.913 | 0 | 4 | 1 | Tab. S1N |
| Zn-ad+1/4-H-e | -65.936 | -65.925 | 0 | 4 | 1 | Tab. S1O |
| Zn-ad+1/4-H-f | -65.924 | -65.913 | 0 | 4 | 1 | Tab. S1P |
| Zn-ad+1/4-H-g | -65.887 | -65.628 | 0 | 4 | 1 | Tab. S1Q |
| Zn-ad+3/8-H | -67.139 | -67.155 | 0 | 6 | 1 | Tab. S1R |
| Zn-ad+1/2-H-a | -68.281 | -68.298 | 0 | 8 | 1 | Tab. S1S |
| Zn-ad+1/2-H-b | -68.305 | -68.324 | 0 | 8 | 1 | Tab. S1T |
| Zn-ad+1/2-H-c | -68.325 | -68.343 | 0 | 8 | 1 | Tab. S1U |
| Zn-ad+O-vac+1/8-H | -48.590 | -48.631 | -1 | 2 | 1 | Tab. S1V |
| ZnO-ad+1/8-H | -80.665 | -80.658 | 1 | 2 | 1 | Tab. S1W |
| ZnO-ad+1/4-H | -81.952 | -81.941 | 1 | 4 | 1 | Tab. S1X |
| ZnO-ad+1/2-H-a | -84.335 | -84.352 | 1 | 8 | 1 | Tab. S1Y |
| ZnO-ad+1/2-H-b | -84.375 | -84.392 | 1 | 8 | 1 | Tab. S1Z |

2 Exploration of the PES of adsorption of CO₂

The calculation of the PES of adsorption of CO₂ on CuZnOpolarO was carried to identify reactive sites. In Fig. S1 the potential energy surfaces (PESs) adsorption of CO₂ are shown for the 1/2-H-sym, 3/8-H-surf, and Zn-ad+1/4-H supported catalyst slab models being relevant to the heterogeneous catalytic process of methanol synthesis from syngas.² Starting from the structures of 1/2-H-sym, 3/8-H-surf, and Zn-ad+1/4-H (see Tab. S1x, Tab. S1t and Tab. S1M) a CO₂ molecule was placed at the vertices of a 16 × 16 × 3 regular grid over the catalyst surface. In the region over the Cu nanoparticle this grid was changed to a regular spherical grid of adequate density. At all grid positions the CO₂ was placed in parallel, perpendicular and upright configuration and the O atoms of the adsorbate were relaxed in the first step, only. Secondly, the whole CO₂ was relaxed for those structures which were closest to the catalyst surface in addition to adsorbate structures that resulted in bent CO₂. Herein, the positions of the atoms of the Cu₈/ZnO(0001) model were kept fixed.

The final PESs of the three catalyst surfaces are depicted in Fig. S1 which displays the different energetics and spatial distribution of CO₂ adsorption. In particular, when looking at the 3/8-H-surf model local minima of adsorption are rather similarly distributed over the ZnO support surface as well as over Cu sites of the metal nanoparticle. The latter site features the global minimum of adsorption with $E_{ads} = -0.66$ eV for CO₂ on this catalyst model. The pictures changes for the catalyst models relevant at more reducing conditions, i.e. 1/2-H-sym and Zn-ad+1/4-H, which show enhanced reactivity on the ZnO support. Adsorption energies of CO₂ on these two models are found as low as -0.44 eV, and -0.42 eV respectively for on top of unsaturated O atoms of the surface layer. We note that these results represent only the adsorption energies of CO₂ over catalyst models with fixed positions of the nuclei, which in the next step were relaxed, too (see next section).

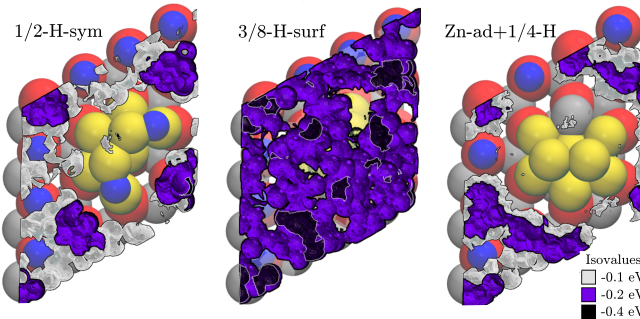


Figure S1 Potential energy surfaces of adsorption of CO_2 built of the set of energies obtained from relaxing CO_2 on many different configurations over the 1/2-H-sym, 3/8-H-surf, and Zn-ad+1/4-H models (see Tab. S1x, Tab. S1t and Tab. S1M) a CO_2 , respectively). A Gaussian broadening was applied for clarity. The color code for the atoms see Tab. S1.

3 Adsorption sites of CO_2 on Cu nanocatalysts supported on $\text{ZnO}(000\bar{1})$

In the final step of our approach we have located the most stable adsorption sites of CO_2 . Starting from the PESs of adsorption of 1/2-H-sym, 3/8-H-surf and Zn-ad+1/4-H surface morphologies (see previous section) we have selected the following structures: (i) with negative adsorption energies or (ii) resulted in an bend CO_2 configuration. Subsequently, a full relaxation of the nuclear positions of all atoms but the lower half of the support was carried out obtain lowest energy structures. In addition to the three catalyst models we also investigated the adsorption behavior of CO_2 on 1/2-H-top and ZnO -ad+1/2-H-b catalyst models. Herein, we followed a simpler route locating the adsorption sites of CO_2 , i.e., we adapted stable adsorption geometries obtained for 1/2-H-sym, and Zn-ad+1/4-H models, respectively. Finally, we summarize the most stable adsorbate structures of CO_2 for all five surface structures 1/2-H-sym, 1/2-H-top, 3/8-H-surf, Zn-ad+1/4-H and ZnO -ad+1/2-H-b models in Tab. S3, Tab. S4, Tab. S5, Tab. S6, and Tab. S7, respectively.

The adsorption energy, $E_{\text{ads}}^{\text{CO}_2}$ of CO_2 molecules on the different $\text{Cu}_8/\text{ZnO}(000\bar{1})$ models was calculated following as usual from

$$E_{\text{ads}}^{\text{CO}_2} = E_{\text{CO}_2 @ \text{cat}}^{\text{KS+vdW}} - (E_{\text{CO}_2}^{\text{KS+vdW}} + E_{\text{cat}}^{\text{KS+vdW}}), \quad (1)$$

with $E^{\text{KS+vdW}}$ corresponding to the Kohn–Sham total energies using the extended k -point sampling scheme plus energetic contributions from the dispersion correction³ to account for van der Waals interactions. Negative values of $E_{\text{ads}}^{\text{CO}_2}$ indicate thermodynamically stable adsorption. The corresponding results of $E_{\text{ads}}^{\text{CO}_2}$ on all five surface structures are summarized in Tab. S8.

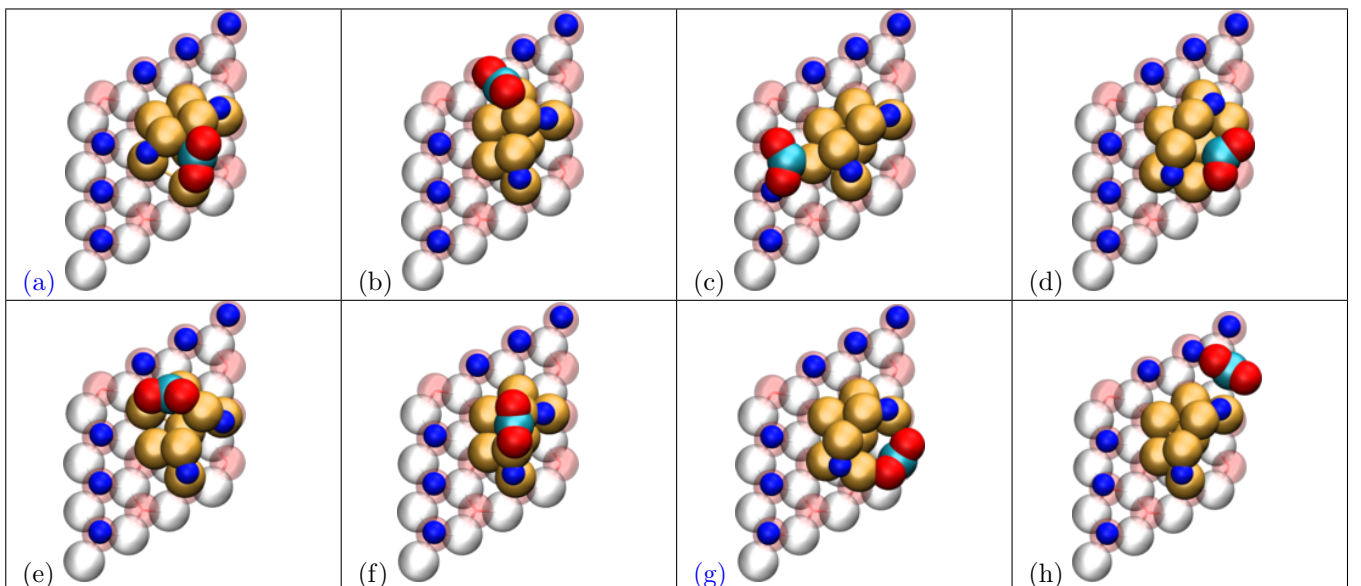


Table S3 Most stable adsorption sites of CO_2 on the 1/2-H-sym catalyst model. Same Color code of the atoms as Tab. S1 plus C-atom (cyan). Blue labels indicate structures that also appear in figures of the main paper.

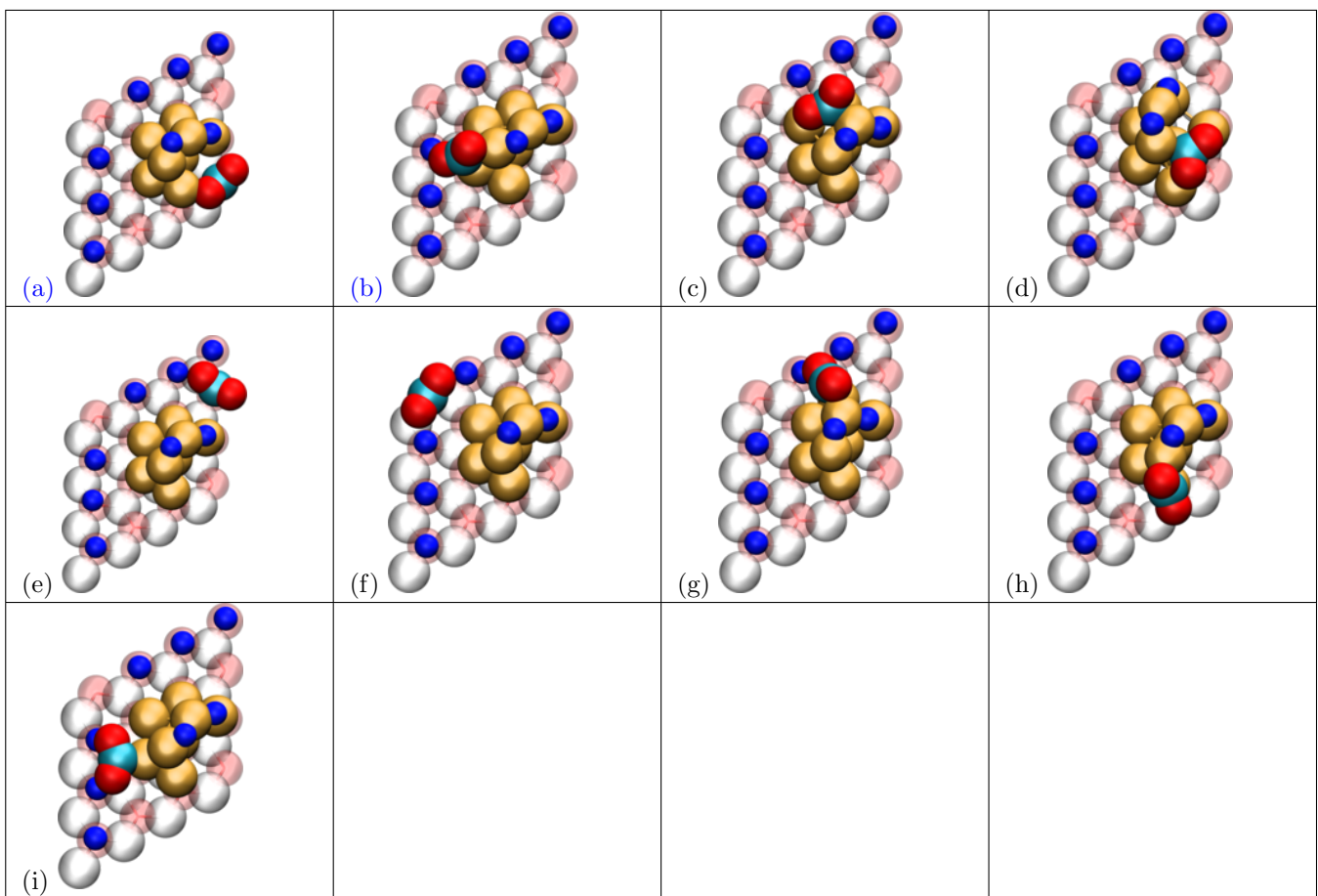


Table S4 Most stable adsorption sites of CO₂ on the 1/2-H-top catalyst model. Same Color code of the atoms as Tab. S1 plus C-atom (cyan). Blue labels indicate structures that also appear in figures of the main paper.

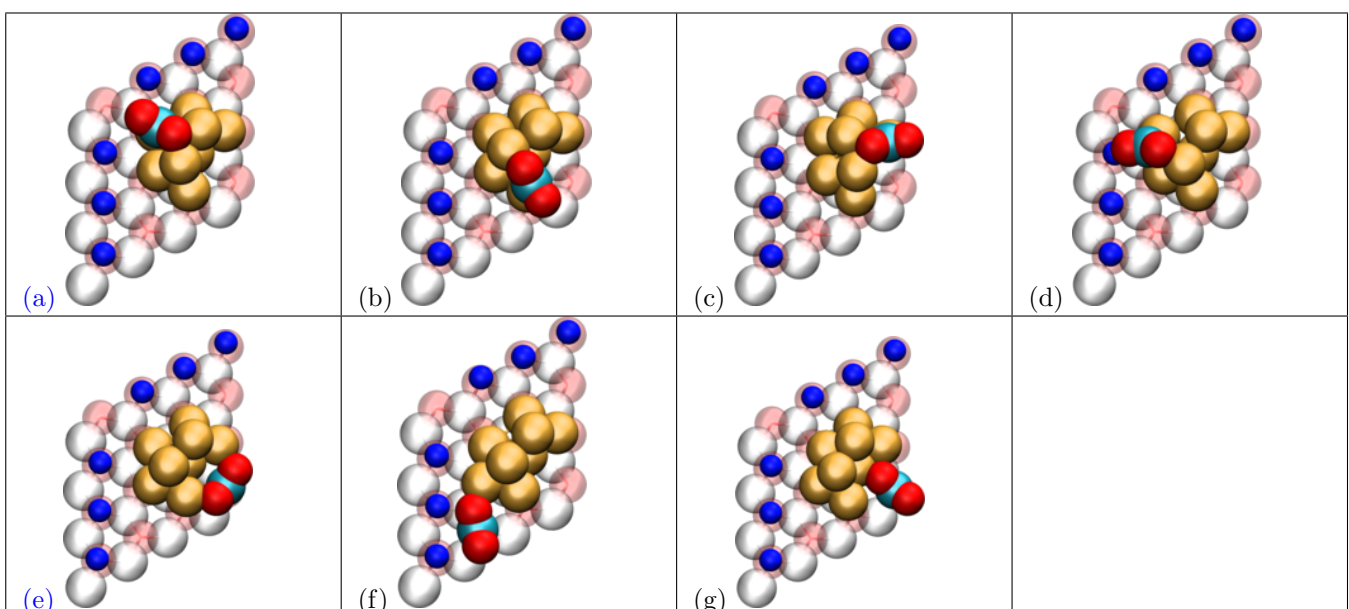


Table S5 Most stable adsorption sites of CO₂ on the 3/8-H-surf catalyst model. Same Color code of the atoms as Tab. S1 plus C-atom (cyan). Blue labels indicate structures that also appear in figures of the main paper.

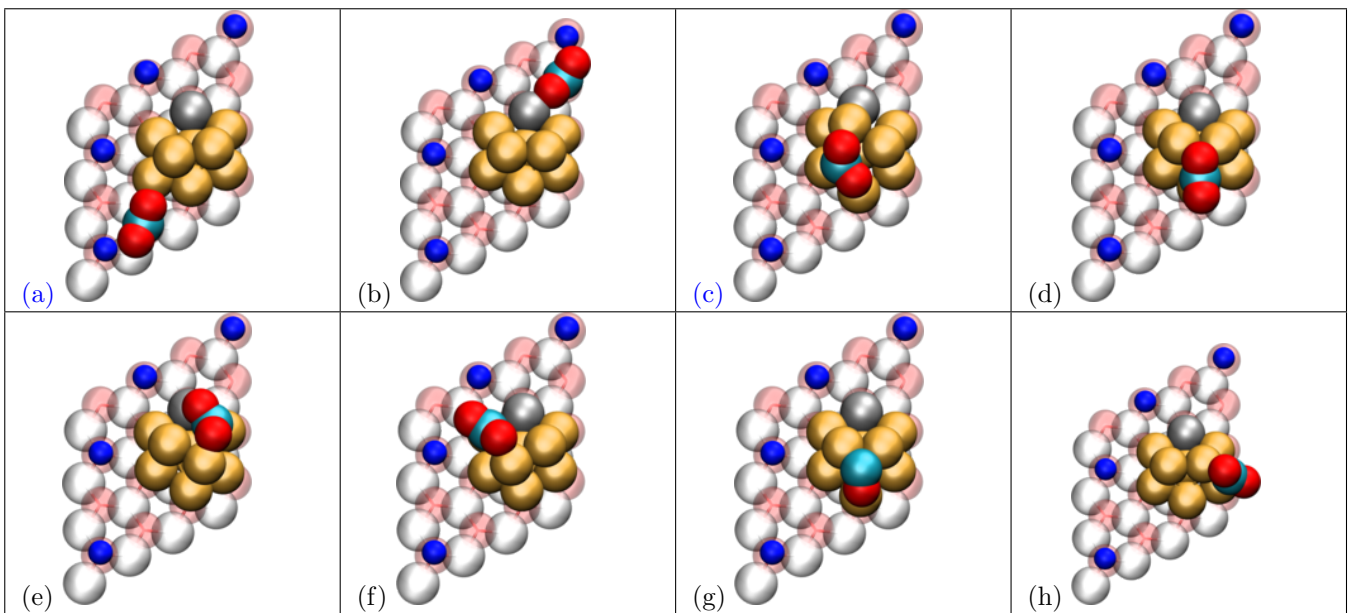


Table S6 Most stable adsorption sites of CO_2 on the Zn–ad+1/4–H catalyst model. Same Color code of the atoms as Tab. S1 plus C-atom (cyan). Blue labels indicate structures that also appear in figures of the main paper.

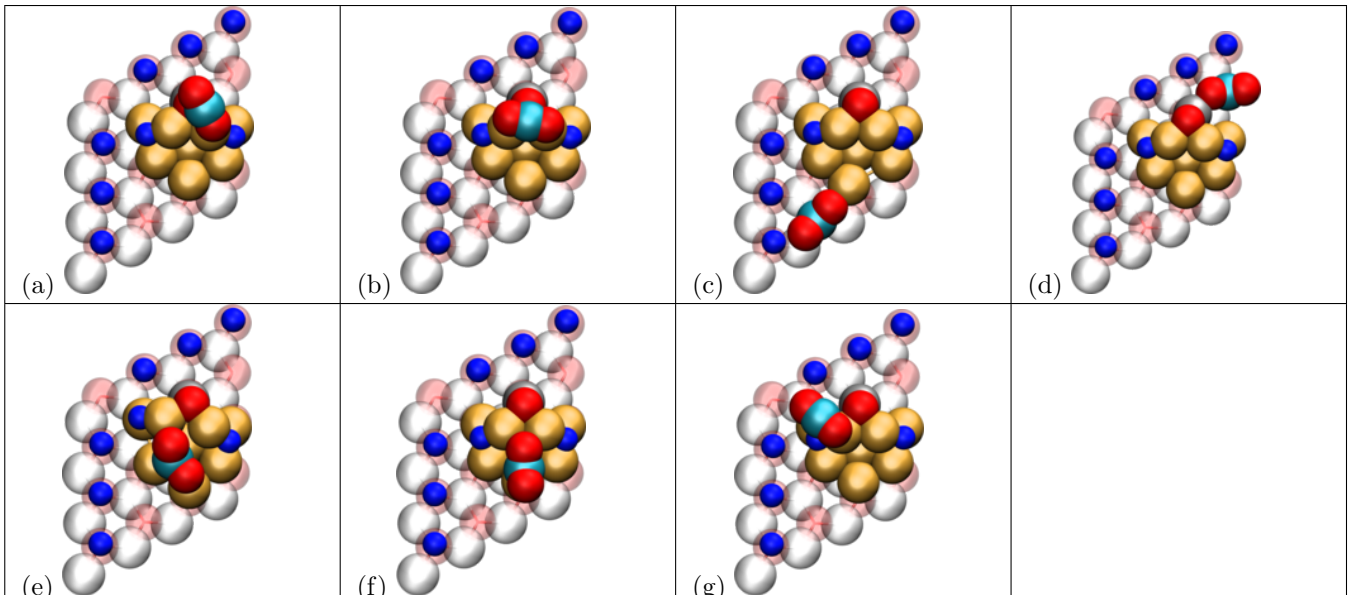


Table S7 Most stable adsorption sites of CO_2 on the ZnO–ad+1/2–H–b catalyst model. Same Color code of the atoms as Tab. S1 plus C-atom (cyan). Blue labels indicate structures that also appear in figures of the main paper.

Table S8 Adsorption energies of CO_2 @Cu/ZnO models. Blue labels indicate structures that also appear in figures of the main paper.

| catalyst model | CO_2 adsorption site | E_{ads} /eV | structure |
|----------------|-------------------------------|----------------------|-----------|
| 1/2–H–sym | Cu ₈ | -1.41 | Tab. S3a |
| 1/2–H–sym | Cu ₈ | -1.28 | Tab. S3b |
| 1/2–H–sym | Cu ₈ | -1.02 | Tab. S3c |
| 1/2–H–sym | Cu ₈ | -0.97 | Tab. S3d |
| 1/2–H–sym | Cu ₈ | -0.93 | Tab. S3e |
| 1/2–H–sym | Cu ₈ | -0.88 | Tab. S3f |
| 1/2–H–sym | O–(ZnO) | -0.82 | Tab. S3g |
| 1/2–H–sym | O–(ZnO) | -0.62 | Tab. S3h |
| 1/2–H–top | O–(ZnO) | -0.83 | Tab. S4a |

Continued on next page

Table S8 – continued from previous page

| catalyst model | CO ₂ adsorption site | E_{ads}/eV | structure |
|----------------|---------------------------------|----------------------------|-----------|
| 1/2-H-top | Cu ₈ | -0.73 | Tab. S4b |
| 1/2-H-top | Cu ₈ | -0.61 | Tab. S4c |
| 1/2-H-top | Cu ₈ | -0.60 | Tab. S4d |
| 1/2-H-top | O-(ZnO) | -0.59 | Tab. S4e |
| 1/2-H-top | O-(ZnO) | -0.58 | Tab. S4f |
| 1/2-H-top | Cu ₈ | -0.58 | Tab. S4g |
| 1/2-H-top | Cu ₈ | -0.47 | Tab. S4h |
| 1/2-H-top | Cu ₈ | -0.45 | Tab. S4i |
| 3/8-H-surf | Cu ₈ | -1.11 | Tab. S5a |
| 3/8-H-surf | Cu ₈ | -0.89 | Tab. S5b |
| 3/8-H-surf | Cu ₈ | -0.89 | Tab. S5c |
| 3/8-H-surf | Cu ₈ | -0.86 | Tab. S5d |
| 3/8-H-surf | O-(ZnO) | -0.85 | Tab. S5e |
| 3/8-H-surf | O-(ZnO) | -0.48 | Tab. S5f |
| 3/8-H-surf | O-(ZnO) | -0.20 | Tab. S5g |
| Zn-ad+1/4-H | O-(ZnO) | -1.09 | Tab. S6a |
| Zn-ad+1/4-H | O-(ZnO) | -1.03 | Tab. S6b |
| Zn-ad+1/4-H | Cu ₈ | -0.84 | Tab. S6c |
| Zn-ad+1/4-H | Cu ₈ | -0.47 | Tab. S6d |
| Zn-ad+1/4-H | Cu ₈ | -0.44 | Tab. S6e |
| Zn-ad+1/4-H | Cu ₈ | -0.42 | Tab. S6f |
| Zn-ad+1/4-H | Cu ₈ | -0.40 | Tab. S6g |
| Zn-ad+1/4-H | Cu ₈ | -0.23 | Tab. S6h |
| ZnO-ad+1/2-H-b | O-(ZnO) + O-(Zn-ad) | -0.96 | Tab. S7d |
| ZnO-ad+1/2-H-b | Cu ₈ | -0.66 | Tab. S7e |
| ZnO-ad+1/2-H-b | O-(ZnO) | -0.73 | Tab. S7c |
| ZnO-ad+1/2-H-b | Cu ₈ | -0.42 | Tab. S7f |
| ZnO-ad+1/2-H-b | Cu ₈ (vdW) | -0.24 | Tab. S7a |
| ZnO-ad+1/2-H-b | Cu ₈ (vdW) | -0.23 | Tab. S7b |
| ZnO-ad+1/2-H-b | Cu ₈ (not bound) | -0.09 | Tab. S7g |

4 Spatial analysis of the redox state of Cu nanoparticle and ZnO support

In order to characterize the redistribution of electronic charge Δq^X between different parts X of two different surface structures (e.g. ZnO support, Cu cluster, and adatoms), we projected⁴ the electronic charge density onto atom-centered electronic populations yielding partial charges $q_i, \forall i \in X$. For example the transfer from or onto the ZnO substrate (i.e. $X = \text{ZnO}$) is calculated following

$$\Delta q^{X=\text{ZnO}} = \sum_{i \in \text{O}, \text{Zn}} (q_i^{\text{cat}} - q_i^{\text{ref}}) , \quad (2)$$

where q_i^{cat} is the electronic population of atom i of the ZnO support of the catalyst model of interest and q_i^{ref} is that of the corresponding atom i of another of our calculated structures acting as reference. When analyzing bare catalyst Cu/ZnO surface structures the 3/8-H-flat model is used exclusively as reference, while in the case of CO₂ adsorption the latter is always represented by the isolated structures of molecular CO₂ and the corresponding free catalyst.

Herein we provide the results of this analysis on the adsorbate dependent the oxidation state of the ZnO support on catalyst structures. In Fig. S2 we plot the results for a large selection fully oxidized and reduced CuZnOpolarO structures with respect to the 1/2-H-sym model see (Fig. S2). Next, we analyzed the charge re-distribution in the ZnO upon the adsorption CO₂ on 1/2-H-sym, 3/8-H-flat, 1/2-H-top, Zn-ad+1/4-H and ZnO-ad+1/2-H-b cluster models. Moreover, following the same procedure the effects of H₂ adsorption and spill-over to the metal particle, O-vacancy creation, partial alloying of Zn into the copper, partial overgrowing of the support onto copper, partial oxidation of copper as well as the desorption of H₂O were carried out for selected examples of catalyst model structures, i.e. see S5, S6, S7, S8, S9, S10 and S11, respectively.

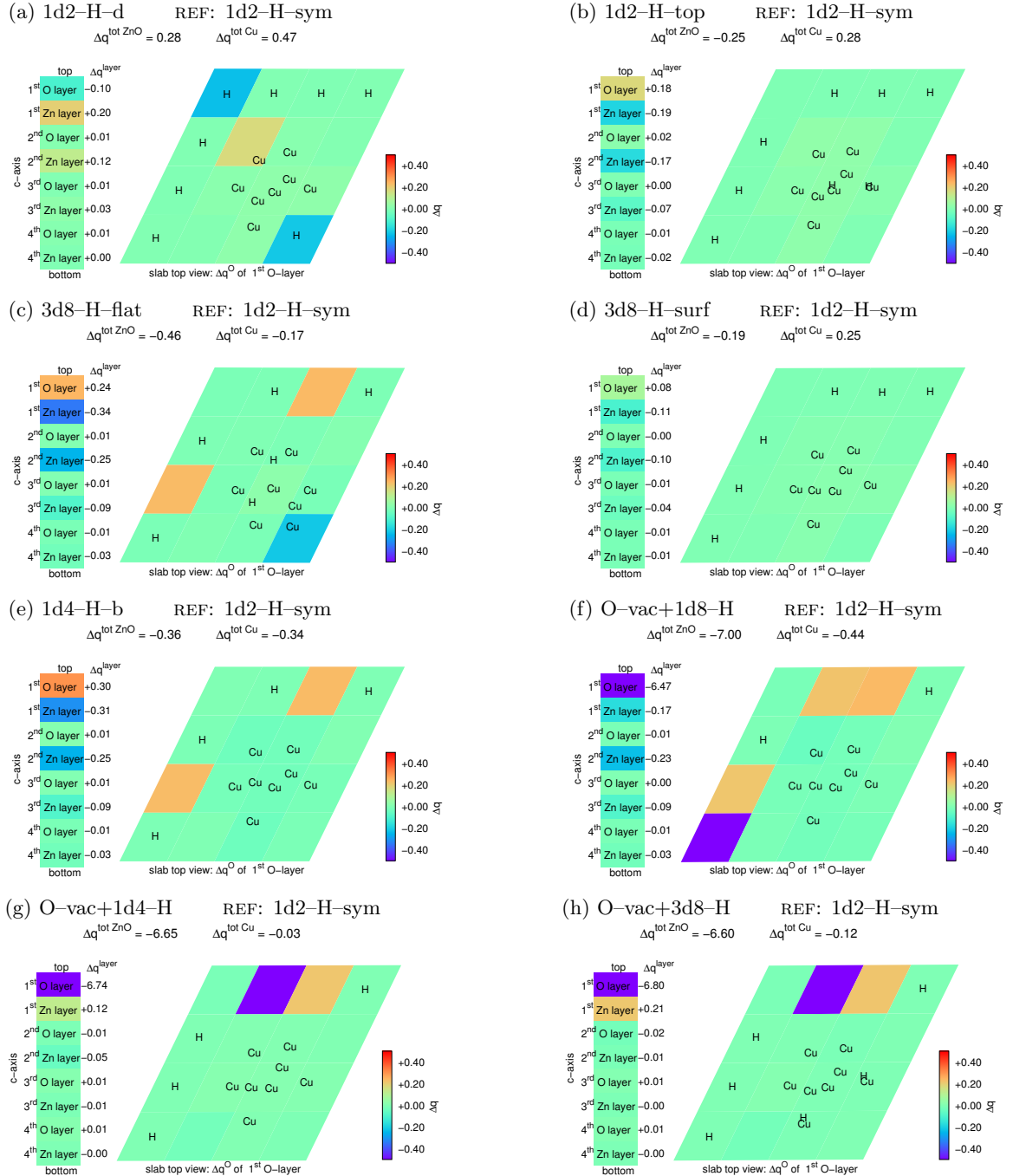


Figure S2 Change of the oxidation state of ZnO support and Cu nanocatalyst. The difference of the electron population of individual atoms, Δq^X , between two Cu/ZnO surface structure is depicted (see Eq. (2)). In all subfigures the same reference structure, 1/2-H-sym, is used. The spatial resolution of Δq is provided for the ZnO substrate and the Cu₈ nanocatalyst by $\Delta q^{\text{tot ZnO}}$ and $\Delta q^{\text{tot Cu}}$, respectively. Moreover, $\Delta q^{\text{tot ZnO}}$ is resolved down to the individual layers of the surface, i.e. the slabs of O atoms and Zn atoms, i.e. Δq^{layer} and Δq^{atom} , respectively, as well as to the O atoms of the surface O layer, i.e. $\Delta q^{\text{O atom}}$ (bottom right of the subfigures). Positive values of Δq (color code: yellow to red) indicate electron accumulation (corresponding chemically to reduction) compared to the reference, while negative values of Δq (color code: cyan to blue) indicate electron depletion (oxidation). The position of atoms of the catalyst structures which are above the O surface layer are indicated by their atom symbols; the atoms of the reference structure are not shown.

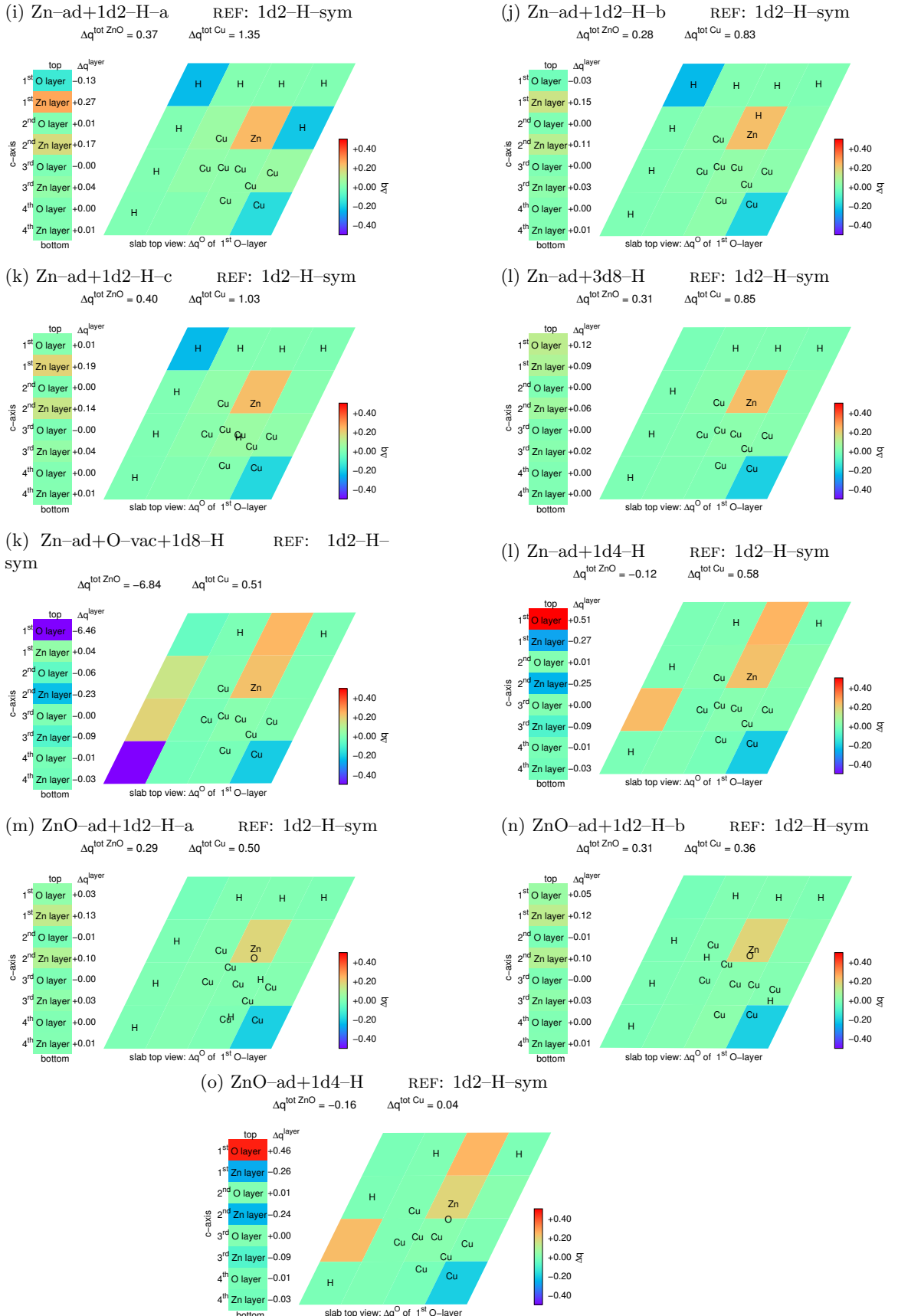


Figure S2 (Continued) Change of the oxidation state of the ZnO support: Difference of the electron population of the individual O and Zn atoms of selected $\text{Cu}_8\text{ZnO}(000\bar{1})$ models and the 1/2-H-sym model acting as reference.

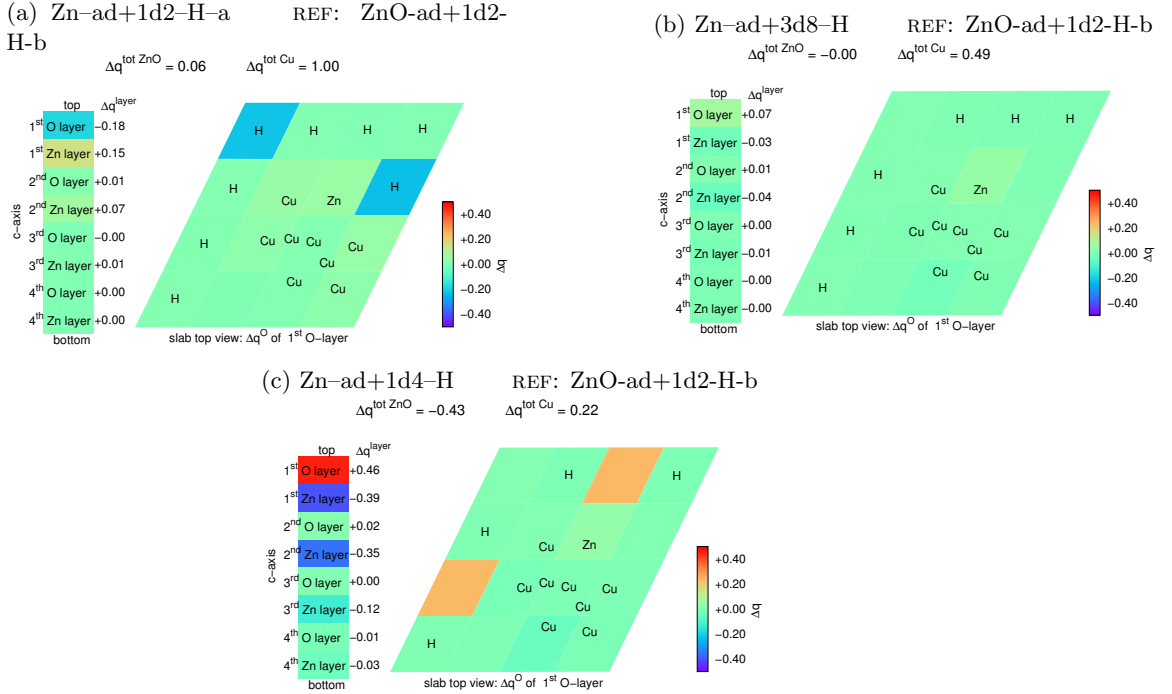


Figure S3 Change of the oxidation state of the ZnO support: Difference of the electron population of the individual O and Zn atoms of selected $\text{Cu}_8\text{ZnO}(000\bar{1})$ models and the ZnO-ad+1d2-H-b (see Tab. S1(Z)) model acting as reference. Further details see Fig. S2

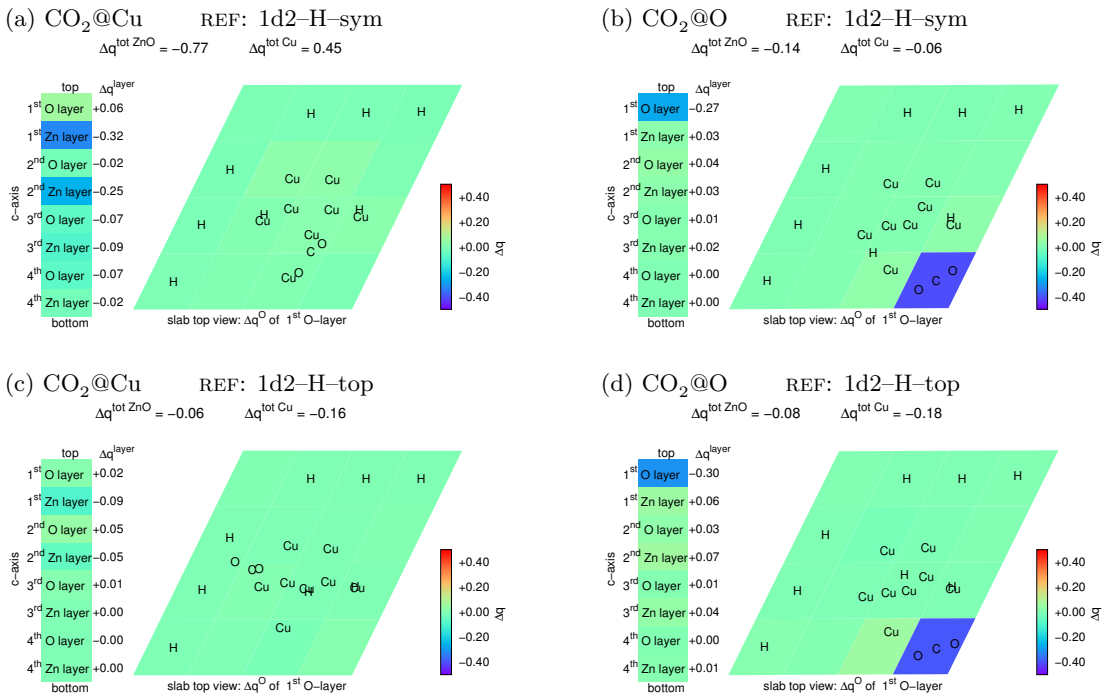


Figure S4 CO_2 adsorption affecting the oxidation state of the ZnO support: Difference of the electron population of the individual O and Zn atoms of $\text{Cu}_8\text{ZnO}(000\bar{1})$ models with CO_2 to the one without CO_2 is shown. The most stable adsorbate structures of CO_2 being adsorbed at the copper cluster (left column) and CO_2 being adsorbed at the ZnO support (right column) are shown. Further details see Fig. S2

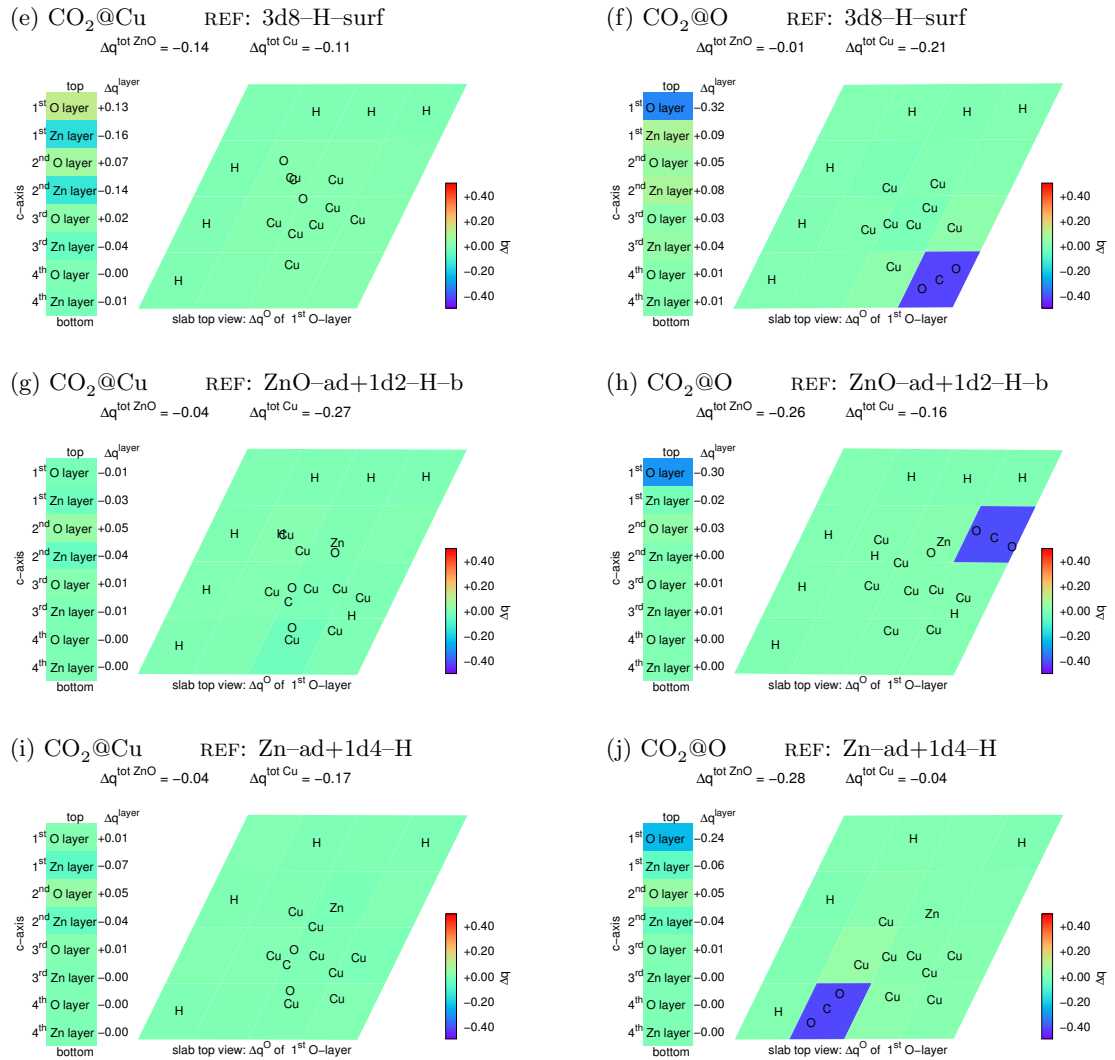


Figure S4 (Continued) CO_2 adsorption affecting the oxidation state of the ZnO support.

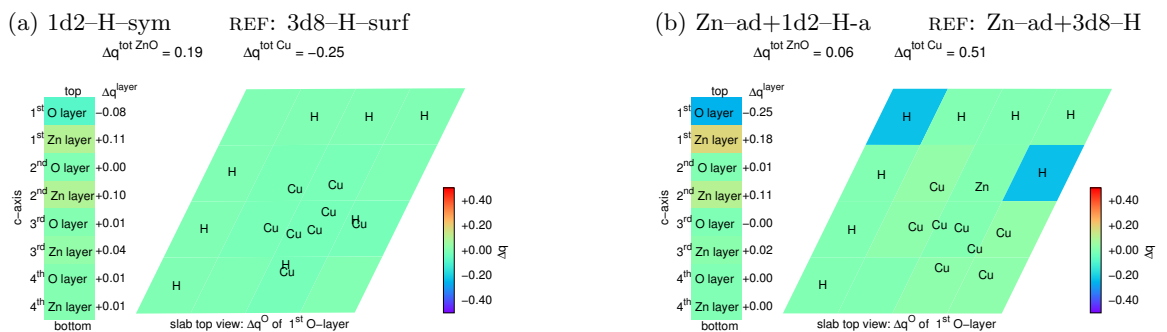


Figure S5 H_2 adsorption affecting the oxidation state of the ZnO support: Difference of the electron population of the individual O and Zn atoms of $\text{Cu}_8\text{ZnO}(000\bar{1})$ models with H_2 to the one without H_2 is shown. The most stable adsorbate structures of H_2 being adsorbed at the copper cluster (left column) and H_2 being adsorbed at the ZnO support (right column) are shown. Further details see Fig. S2

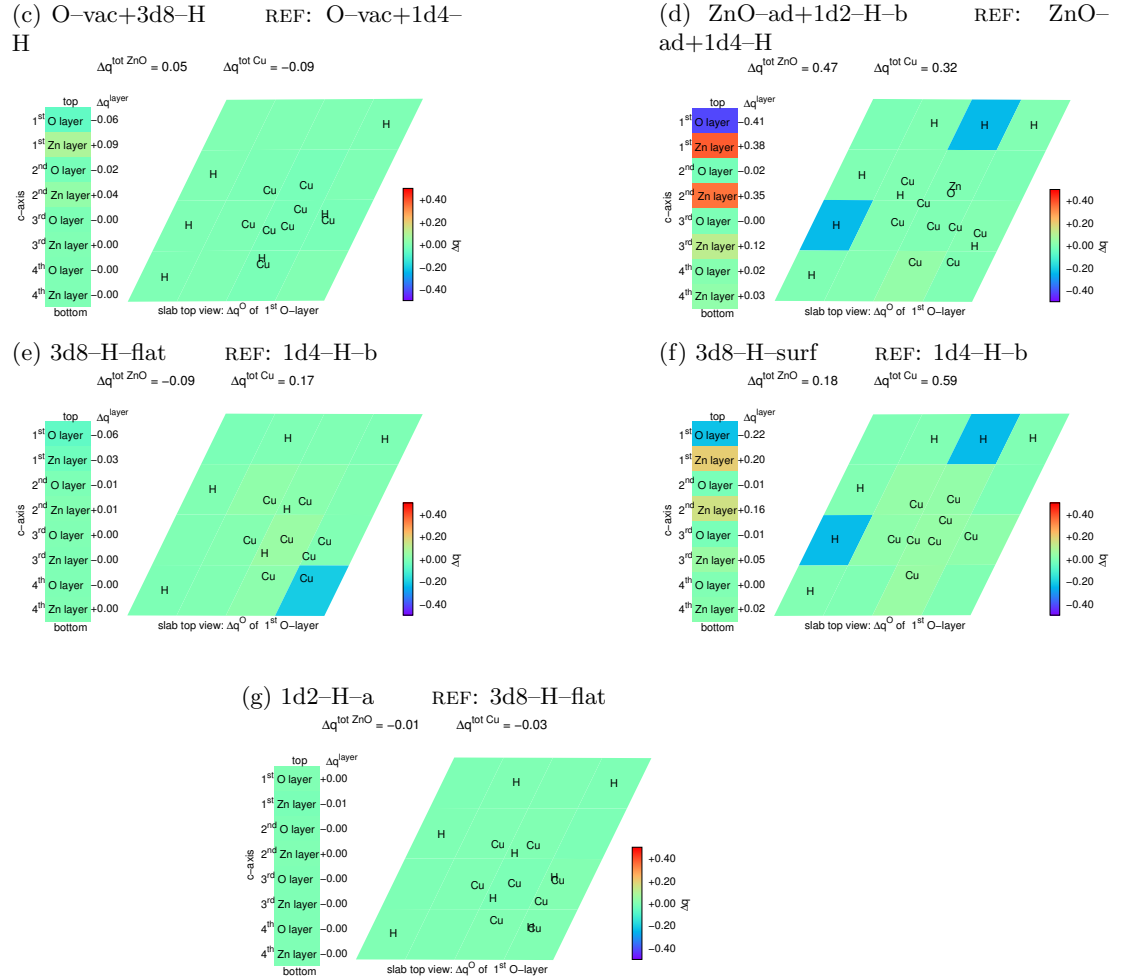


Figure S5 (Continued) H_2 adsorption affecting the oxidation state of the ZnO support.

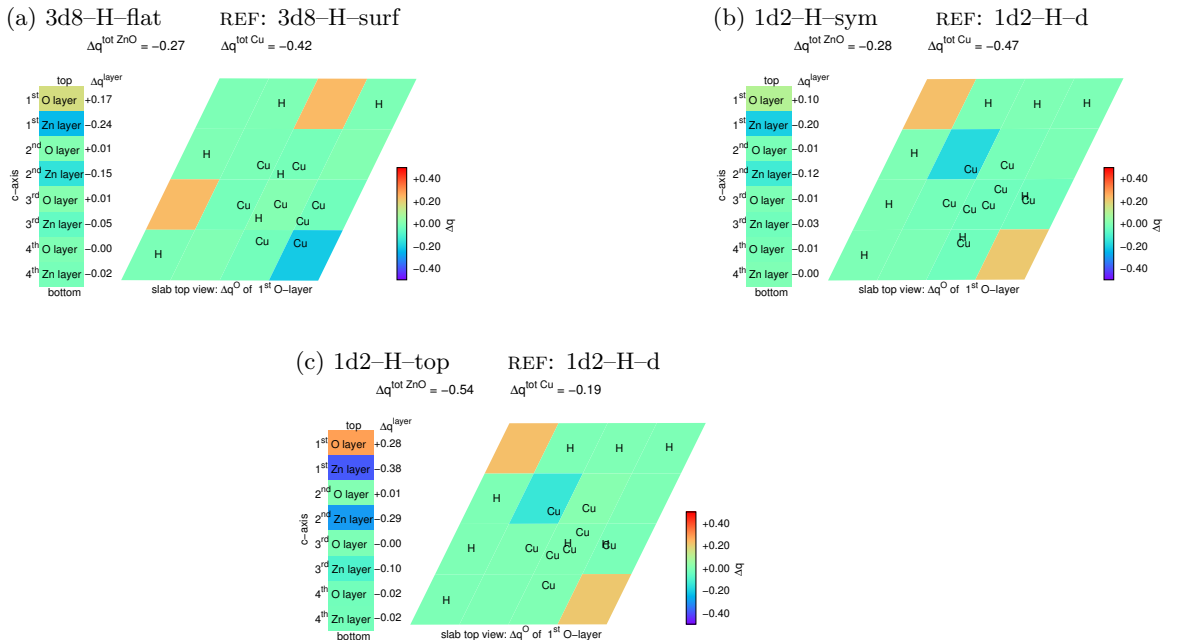


Figure S6 H spillover to copper affecting the oxidation state of the ZnO support: Difference of the electron population of the individual O and Zn atoms of $\text{Cu}_8\text{ZnO}(000\bar{1})$ models with H atoms at the copper cluster to the one with the H at the O atoms of the support is shown. Further details see Fig. S2

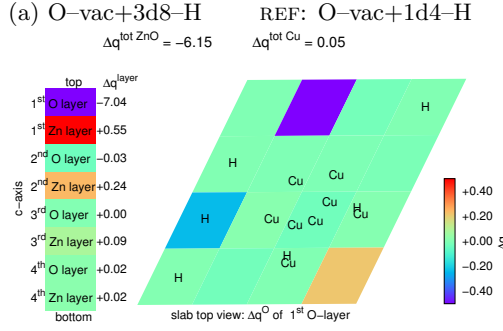


Figure S7 O vacancies affecting the oxidation state of the ZnO support: Difference of the electron population of the individual O and Zn atoms of $\text{Cu}_8\text{ZnO}(000\bar{1})$ models with a O vacancy the one without it is shown. Further details see Fig. S2

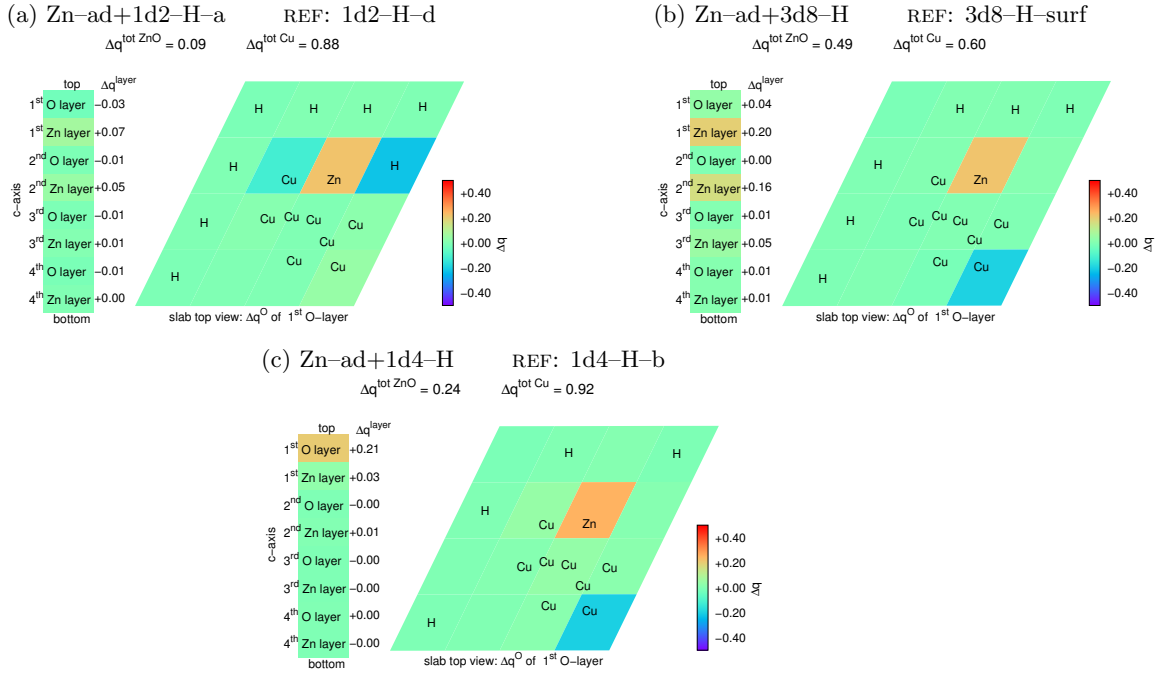


Figure S8 Zn alloying affecting the oxidation state of the ZnO support: Difference of the electron population of the individual O and Zn atoms of $\text{Cu}_8\text{ZnO}(000\bar{1})$ models with Zn to the one without it is shown. Further details see Fig. S2

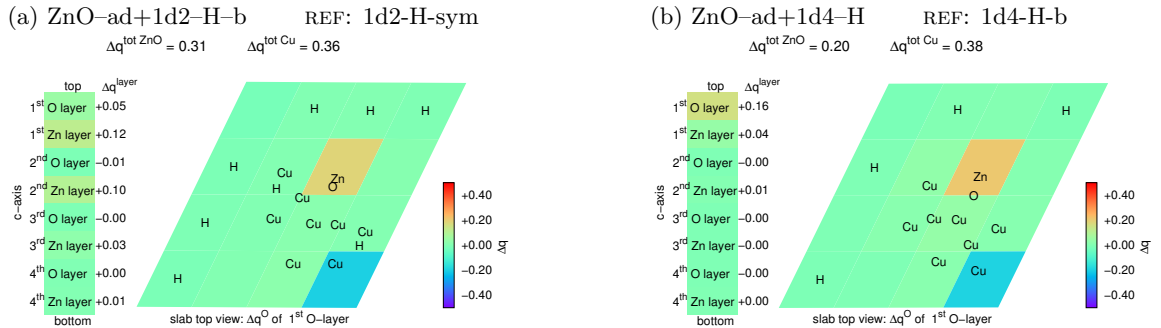


Figure S9 Overgrowing ZnO affecting the oxidation state of the ZnO support: Difference of the electron population of the individual O and Zn atoms of $\text{Cu}_8\text{ZnO}(000\bar{1})$ models with a ZnO-dimer to the one without it is shown. Further details see Fig. S2

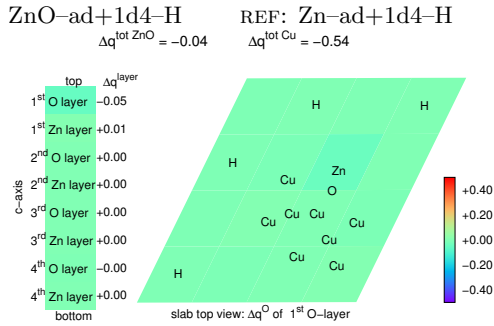


Figure S10 O spillover affecting the oxidation state of the ZnO support: Difference of the electron population of the individual O and Zn atoms of $\text{Cu}_8\text{ZnO}(000\bar{1})$ models with a O atom to the one without it is shown. Further details see Fig. S2

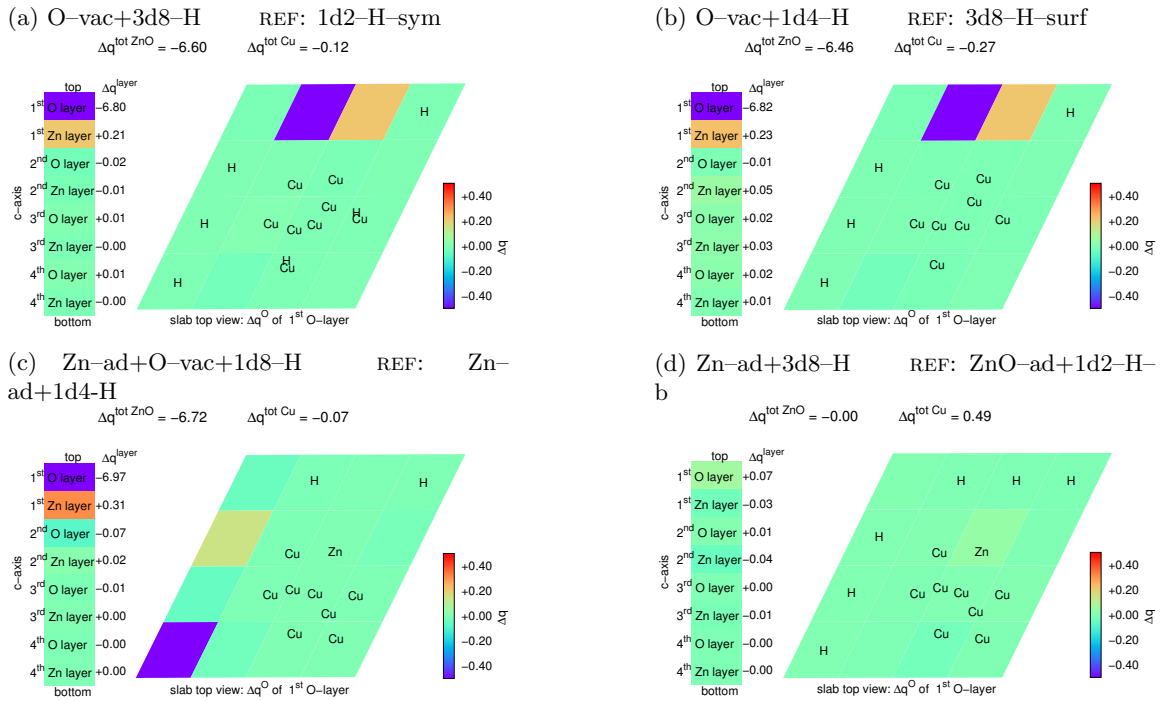


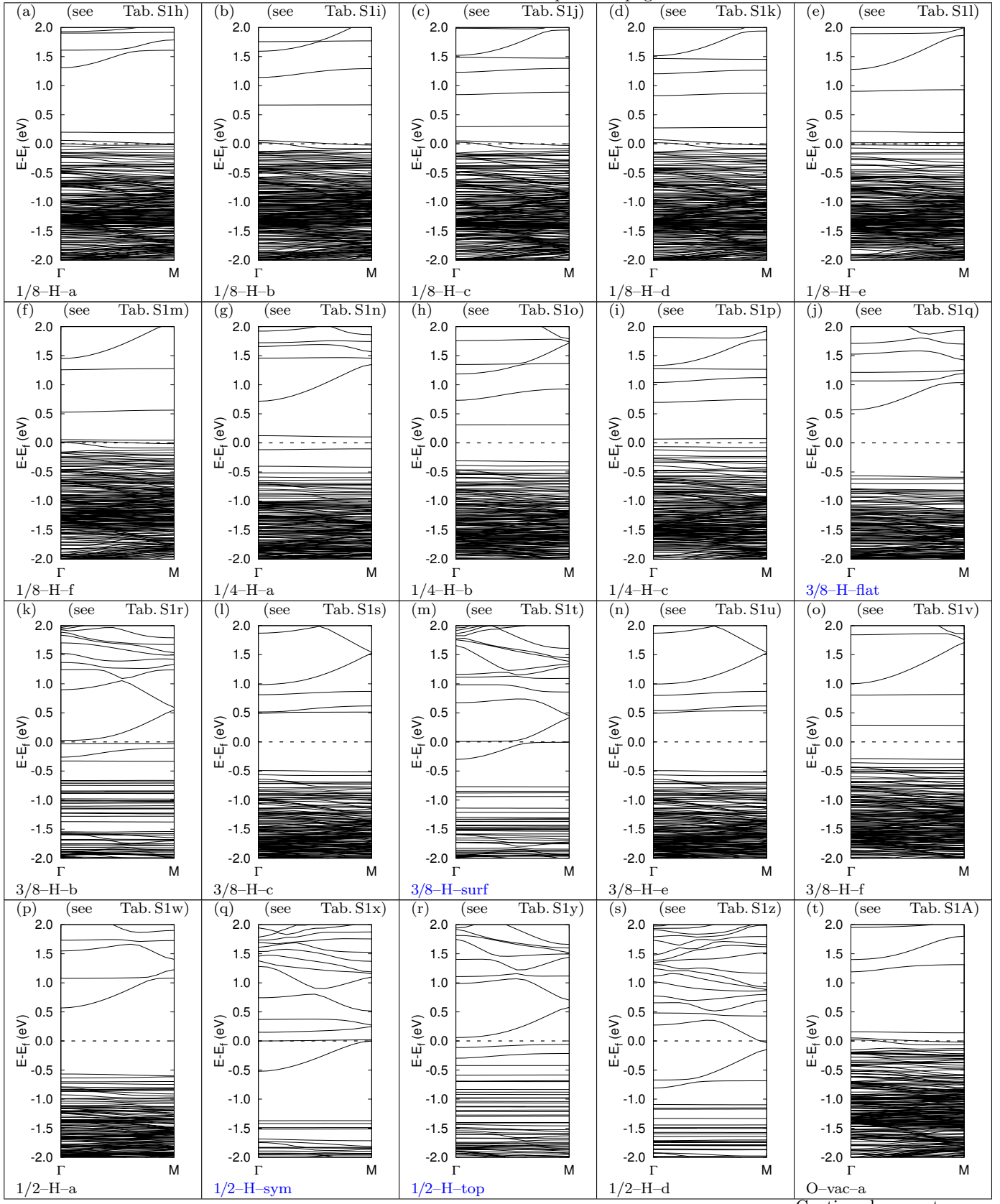
Figure S11 H_2O desorption affecting the oxidation state of the ZnO support: Difference of the electron population of the individual O and Zn atoms of $\text{Cu}_8\text{ZnO}(000\bar{1})$ models without H_2O to the one with H_2O is shown. The most stable adsorbate structures of H_2O desorbed from the copper cluster (lower row) and H_2O desorbed from the ZnO support (upper row) are shown. Further details see Fig. S2

5 Electronic band structures of Cu/ZnO catalyst models

Table S9 Electronic band structure of Cu/ZnO catalyst models. Blue labels indicate structures that also appear in figures of the main paper.

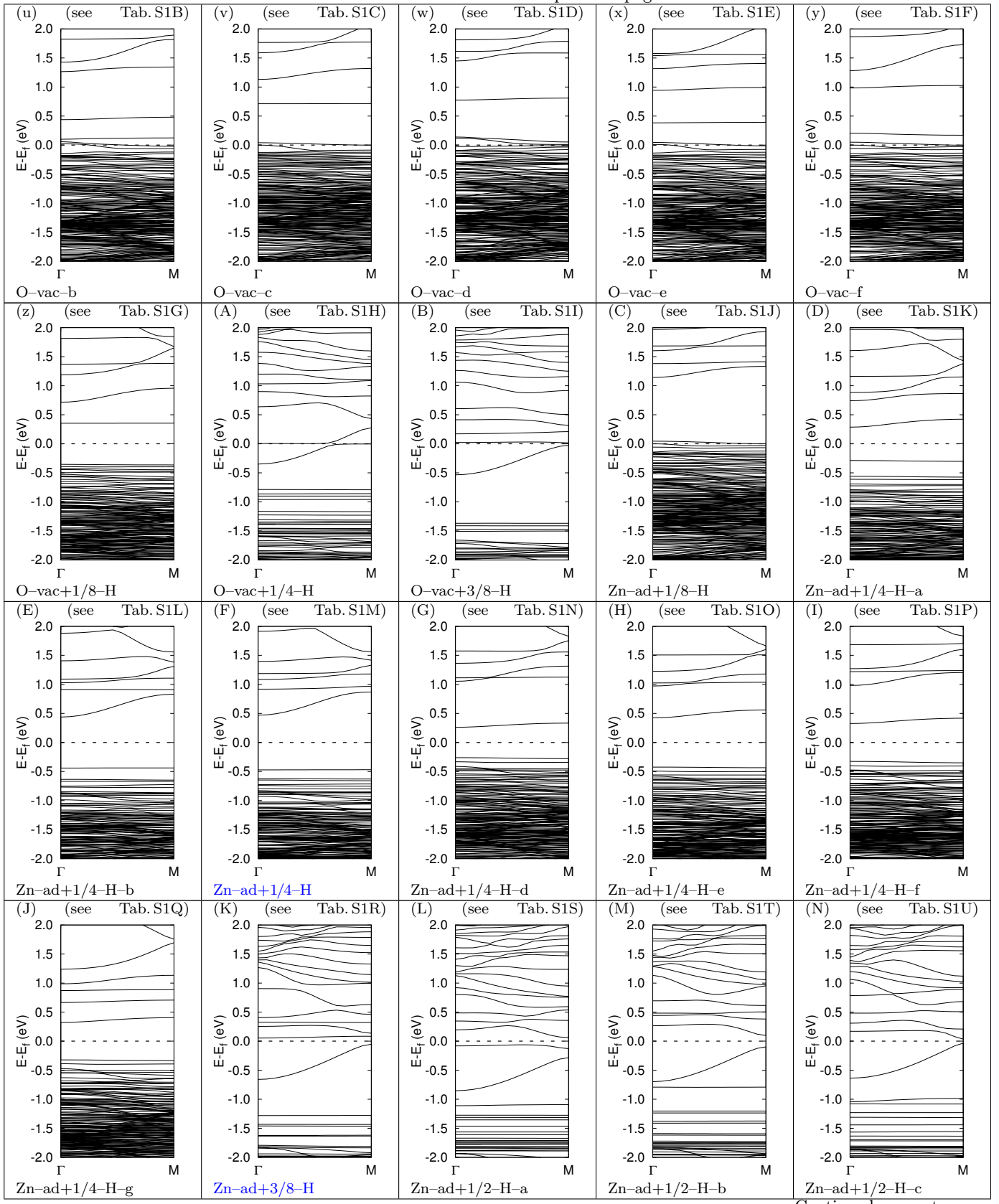
Continued on next page

Table S9 – continued from previous page



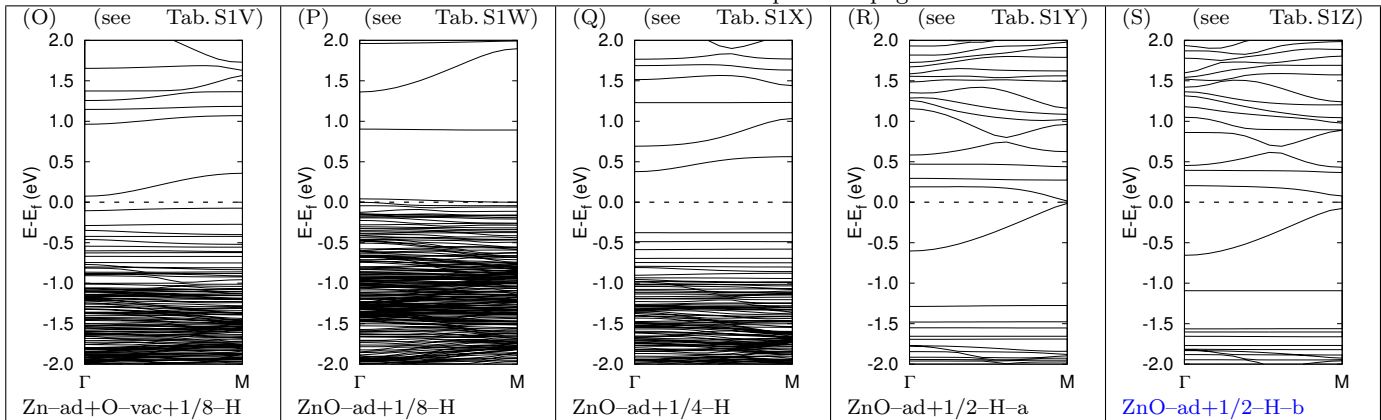
Continued on next page

Table S9 – continued from previous page



Continued on next page

Table S9 – continued from previous page



6 Exploration of CO₂ adsorption sites

We start the discussion with CO₂ being adsorbed at the reduced Cu cluster of Zn-ad+1/4-H which is supported on oxidized ZnO (see Fig. S12a and Fig. 4g of the main paper). Primarily, the presence of the adsorbate does not introduce a qualitative change in the BS, i.e. the large band gap is maintained. Only the states belonging to the metal cluster are lowered in energy which can be explained by the more favorable distribution of the reducing excess charge on the CO₂ rather than dangling bonds of surface Cu atoms of the adsorbate free structure. Accordingly, in the pDOS a cluster state at -0.4 eV shows a significant mixing with contributions stemming

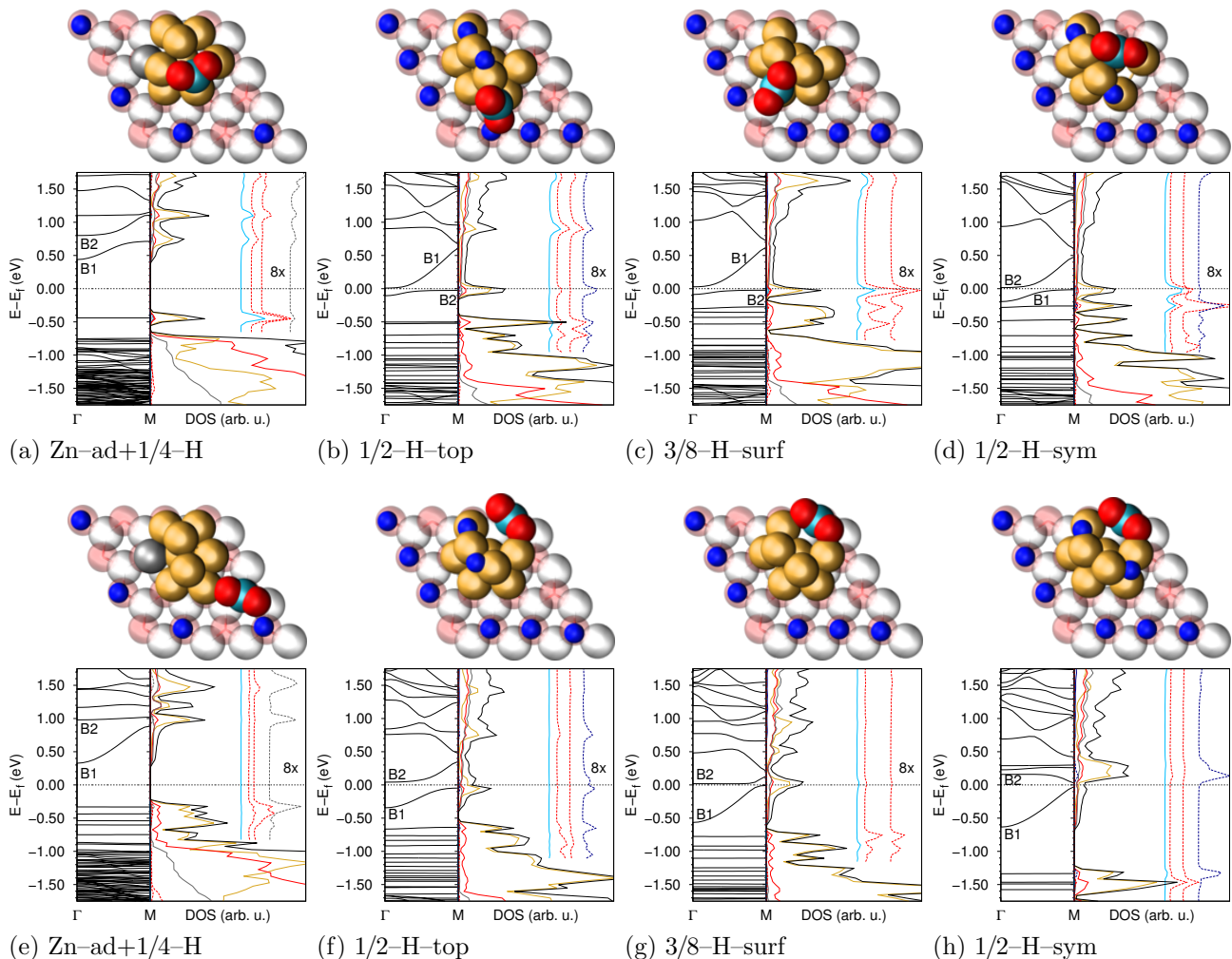


Figure S12 Structure, electronic band structure, and DOS of most stable adsorption sites of CO₂ on four Cu/ZnO catalyst models with each showing Cu cluster and ZnO surface site, see subfigures (a)-(d) and (e)-(h), respectively. Note that all these structures have been fully optimized within our slab model. For the full list of all calculated CO₂ adsorption sites see Tab. 3 to Tab. 7. The nomenclature and color code is the same as that used in Tab. 1. In addition, C atoms are shown in light blue. The BS of subfigure (e) was adopted from Ref. 2.

from the CO₂ species. Similar stabilizing effects on the electronic states of the cluster are present for CO₂ adsorption on Cu of 1/2-H-top exhibiting a more reduced ZnO surface than Zn-ad+1/4-H (see Fig. S12b and Fig. 4g of the main paper). Energy and occupation of the characteristic bands at the Fermi level, B1 and B2, hardly change with respect to the adsorbate-free structure, which explains the absence of a significant charge transfer through the Cu/ZnO interface upon CO₂ adsorption.

The situation changes when CO₂ is activated on more oxidized Cu clusters being supported on a reduced ZnO substrate, i. e. 3/8-H-surf and 1/2-H-sym, which have partially occupied bands B1 located directly at the Fermi energy. Upon CO₂ adsorption these bands become partially emptied while, in turn, localized cluster states B2 are lowered in energy and receive the electrons of these ZnO surface bands B1 (see Fig. S12c and Fig. 4e of the main paper and Fig. S12d and Fig. 4f of the main paper, respectively). As a consequence of this relocation of electronic charge numerous occupied Cu states are shifted closer to the Fermi energy where these orbitals contribute to the binding of the adsorbate as shown in the corresponding plot of the pDOSs.

In stark contrast, the direction of the charge transfer inverts if CO₂ is adsorbed on the ZnO substrate, which can also be understood from the calculated electronic structure (see Fig. S12e-Fig. S12h). The BSs of 1/2-H-sym, 3/8-H-surf, 1/2-H-top, and, Zn-ad+1/4-H feature a general energetic stabilization of surface bands over the state localized at the Cu cluster compared to the corresponding CO₂-free Cu/ZnO structures. However, in this process a spatial redistribution of charge is only possible for those surface structures with a low-lying B1 band at the Fermi energy, i. e. being realized by a higher concentration of 3/8 ML H on the substrate which can accept these electrons. This type of band-filling is realized in 1/2-H-sym and 3/8-H-surf, or, 1/2-H-top with the dispersed band B1 becoming fully or partially occupied, respectively. Further reduction of the ZnO is apparently not possible for Zn-ad+1/4-H. Because of the lower concentration of 1/4 ML H on the substrate, B1 is much higher than the Fermi energy which cannot be compensated by the stabilizing effects on ZnO surface bands after CO₂ adsorption (see Fig. S12e). Besides these general effects on the BS, the adsorption of the carbonate-like species next to the clusters and the formation of contacts between Cu and O of the adsorbate leads to a small mixing of electronic contributions of the latter to the highest occupied Cu states (see pDOS's in Fig. S12e-h). However, the proximity to the Cu cluster does not lead to significant electronic participation of C states in this energy range, thus demonstrating chemically less activity compared to bent CO₂ that is directly bound to the metal.

7 Validation of the electronic structure method

In this study we have employed the computationally efficient PBE generalized gradient approximation^{5,6} (GGA), i. e. a purely semilocal functional, to account for exchange–correlation contributions beyond the local density approximation (LDA). This treatment has been shown previously to correctly reproduce structures and energetics of polar ZnO surfaces⁷ in addition to Cu growth on such surfaces,⁸ which both is of key relevance to the current investigation. Nonetheless, PBE predicts the localized Zn 3d valence states to be at about 3 eV higher in energy compared to the experimental value.^{9,10} Therefore, hybridization with the O 2p states occurs, which leads to an unphysical shift of the valence band of ZnO to higher energies. As a consequence, the experimental band gap of 3.4 eV is largely underestimated by the calculation, i. e. PBE yields only 0.74 eV, but this can be significantly improved by using methods which correct for the self-interaction error inherent in GGA and LDA functionals (see e. g. Refs. 11, 12 and 13 for a few out of many publications that deal with this topic).

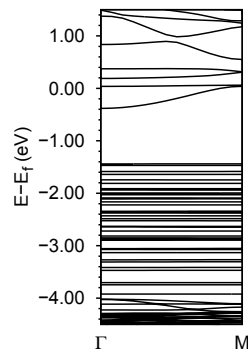


Figure S13 Electronic band structure of the 1/2-H-sym Cu₈/ZnO catalyst model (see text) calculated using a Hubbard U correction, PBE+U. For the Zn 3d and the O 2p states U parameters of 10 eV and 7 eV, respectively, are applied (see text). The remaining computational details are identical to those used for the other plain PBE band structure calculations. The Fermi level is set to zero.

Therefore, using the Hubbard U approach¹⁴, we have performed reference electronic structure calculations thus using PBE+U for our Cu₈/ZnO model. There exist several schemes how to obtain the U parameter. A state-

of-the-art self-consistent approach¹⁵ resulted in $U_{Zn-d}=0$ eV because of the completely filled Zn 3d shell which does not allow a further increase of the occupation of this state. An alternative approach where the parameter U is obtained from first principle calculations underestimates the band gap energy by far.¹³ Therefore we decided to use U parameters which reproduce the experimental band gap energy, i. e. $U_{Zn-3d}=10$ eV and $U_{O-2p}=8$ eV, in order to perform reference calculations for the present purpose.

The calculated band structure employing these U values for the 1/2-H-sym catalyst model, which is relevant at conditions of methanol synthesis, is depicted in Fig. S13. Comparing to the plain PBE band structure (see Fig. 4f of the main paper) we find almost identical band energies in the region around the Fermi level. This particularly holds for the high-lying Cu states and the ZnO conduction band, which facilitate the electronic charge transfer via the Cu/ZnO interface.² This demonstrates that PBE is well suited for the purpose of our study and can be employed to calculate electronic charge distributions for our Cu₈/ZnO catalyst models. Needless to say that it would be highly desirable to use more sophisticated functionals than GGAs, avoiding self-interaction artifacts and properly including dispersion interactions. However, such sophisticated electronic structure approaches are still not practical if accelerated *ab initio* molecular dynamics sampling of catalytic surface chemical reactions – requiring millions of “on the fly” electronic structure calculations to generate the trajectory – is the ultimate goal.^{16–18}

References

- [1] H. J. Monkhorst and J. D. Pack, *Phys. Rev. B*, 1976, **13**, 5188–5192.
- [2] L. Martínez-Suárez, J. Frenzel, D. Marx and B. Meyer, *Phys. Rev. Lett.*, 2013, **110**, 086108.
- [3] S. Grimme, *J. Comput. Chem.*, 2006, **27**, 1787–1799.
- [4] P.-O. Löwdin, *J. Chem. Phys.*, 1950, **18**, 365–375.
- [5] J. P. Perdew, K. Burke and M. Ernzerhof, *Phys. Rev. Lett.*, 1996, **77**, 3865–3868.
- [6] J. P. Perdew, K. Burke and M. Ernzerhof, *Phys. Rev. Lett.*, 1997, **78**, 1396.
- [7] B. Meyer and D. Marx, *Phys. Rev. B*, 2003, **67**, 035403.
- [8] B. Meyer and D. Marx, *Phys. Rev. B*, 2004, **69**, 235420.
- [9] R. Girard, O. Tjernberg, G. Chiaia, S. Söderholm, U. Karlsson, C. Wigren, H. Nylén and I. Lindau, *Surf. Sci.*, 1997, **373**, 409 – 417.
- [10] W. Göpel, J. Pollmann, I. Ivanov and B. Reihl, *Phys. Rev. B*, 1982, **26**, 3144–3150.
- [11] F. Labat, I. Ciofini and C. Adamo, *J. Chem. Phys.*, 2009, **131**, 044708.
- [12] J. Uddin and G. E. Scuseria, *Phys. Rev. B*, 2006, **74**, 245115.
- [13] A. Janotti, D. Segev and C. G. Van de Walle, *Phys. Rev. B*, 2006, **74**, 045202.
- [14] V. I. Anisimov, J. Zaanen and O. K. Andersen, *Phys. Rev. B*, 1991, **44**, 943–954.
- [15] H. J. Kulik and N. Marzari, *J. Chem. Phys.*, 2010, **133**, 114103.
- [16] J. Kiss, J. Frenzel, N. N. Nair, B. Meyer and D. Marx, *J. Chem. Phys.*, 2011, **134**, 064710.
- [17] J. Frenzel, J. Kiss, N. N. Nair, B. Meyer and D. Marx, *Phys. Status Solidi B*, 2013, **250**, 1174–1190.
- [18] J. Frenzel and D. Marx, *J. Chem. Phys.*, 2014, **141**, 124710.